Int. J. Heat Mass Transfer. Vol. 16, pp. 443–460. Pergamon Press 1973. Printed in Great Britain

HEAT TRANSFER FOULING THROUGH GROWTH OF CALCAREOUS FILM DEPOSITS

T. R. GALLOWAY*

Shell Development Company, Emeryville, California, U.S.A.

(*Received* 8 *February* 1972 *and in revised form* 16 *June* 1972)

Abstract—The fouling of heat-transfer equipment surface area results in the equipment being overdesigned some 30 per cent. This added metal and size costs the United States about $400 million dollars per year. Consequently, there is a great incentive to better predict the growth of deposits or films on surfaces.

The growth of calcareous deposits on metal surfaces is predicted through the application of fundamental principles of fluid mechanics and forced convective mass transfer of dissolved oxygen in water. The film thickness was the single most important variable affecting surface transport rate and growth distribution. The idealized case of a bare cylinder maintained at a constant surface concentration with a diffusion barrier series with the concentration boundary layer is taken as the model. Experimentally the growth of the diffusion barrier with time and the complicating effects of hydrodynamics were studied in the laboratory using spherical electrodes placed in a flowing sea water system. The model is used to predict the experimentally measured current decay.

NOMENCLATURE

A, surface area;

C, time averaged concentration [lbspecie/ft^3];

C_P, isobaric heat capacity [cal/gmole°C or Btu/lbmole°F];

C_p, pressure coefficient $= (P_0 - P_\infty)/(1/2\rho_\infty U_\infty^2)$;

$\mathscr{D}$, binary diffusion coefficient (from Chapman–Cowling) [cm^2/s or ft^2/s];

d, diameter of body [cm or ft];

Fs, Frossling group defined by Nu or $Sh/Re^{\frac{1}{2}}Sc^{\frac{1}{3}}$ for cylinders and Nu or $(Sh - 2)/Re^{\frac{1}{2}}Sc^{\frac{1}{3}}$ for spheres;

$\mathscr{F}$, Faraday's constant (96 520 as/equivalent);

g, local acceleration of gravity [cm/s^2 or ft/s^2];

I, longitudinal turbulence of the free stream defined as $[(u')^2]/U_\infty$;

i, current flow [A];

J, current density [A/cm^2];

k, thermal conductivity [cal/scm°C or Btu/sft°F];

K, mass-transfer coefficient $= N/A(C_0 - C_\infty)$ [ft/s];

N, mass flux [g/s or lbm/s];

n, number of equivalents per mole;

P, total pressure [atm];

R_f, fouling resistance [s^{-1} for mass transfer or hft^2°F/Btu for heat transfer];

Re, Reynolds group $= U_\infty d/\nu$;

r, R, radial coordinate [cm or ft];

Sc, Schmidt group $= \nu/\mathscr{D}$;

Sh, time averaged Sherwood group $= kd/\mathscr{D}$;

T, absolute temperature [°K or °R];

t, instantaneous absolute temperature [°K or °R];

T', temperature fluctuations about T [°K or °R];

t, time [s];

U, time averaged velocity in the x direction [cm/s or ft/s];

U_1, velocity in the x direction immediately outside the boundary layer [cm or ft];

u, instantaneous velocity in the x direction [cm/s or ft/s];

u', velocity fluctuations about U [cm/s or ft/s];

x, component coordinate [cm or ft];

* Presently at the University of California, Berkeley, California.

y, component coordinate [cm or ft].

Greek

α, thermal diffusivity, $K/\rho\, C_p$ [cm^2/s];

ε, eddy coefficient [cm^2/s];

μ, viscosity of the media at position x, y, z [g/fts or lbm/fts];

ξ, dimensionless film thickness, $\frac{1}{2}\,\mathrm{Ln}\,(r_1/r_0)$;

ρ, density of the media at position x, y, z [g/cm^3 or lbm/ft^3].

Subscripts

A, molecular specie A;

B, molecular specie B;

d, of diffusion;

eff, effective quantity;

∞, in the free stream.

1. INTRODUCTION

THE PROBLEM of fouling of heat-transfer equipment is widespread in many industries and results in equipment being overdesigned some 30 per cent. The cost of this overdesign in the United States is around $400 million dollars per year. The subject of fouling has not been adequately organized into areas of sufficiently well defined problems and as a result no serious academic research programs have been directed to the subject. Classical texts on heat transfer have done no more than introduce the subject.

Recently Taborek *et al.* [1] organized the problems in heat-transfer fouling and summarized the available literature. In terms of their identified fouling mechanisms the present model may be useful for fouling involving crystallization, sedimentation, chemical reaction, organic material growth or corrosion mechanisms. This model is different than any summarized by Taborek *et al.* in that the film growth rate is dependent upon the diffusional resistance through the film and the mass transfer boundary layer outside the film; with the resistances taken in series. This concept is applicable to the class of fouling problems where a deposit is formed as a result of a reactive component diffusing through the film barrier and reacting with another component appearing at the surface (metal) in excess.

The phenomena responsible for the deposits building up on the surface in a film layer for this particular case of calcareous film appears to be one involving heterogeneous crystallization, although the experimental facts might also be explained by electrokinetic processes acting between a precipitate nucleus formed by homogeneous nucleation from supersaturation and the surface film. Such electrokinetic behavior has been presented [2] as an explanation for observed heat transfer fouling in power stations. In the present case the higher conductivity of the salt water would greatly reduce the range of the electrostatic force field but would increase the field strength. In this way, velocity effects on the electric double layer should not be as significant as in power plant fouling. For this problem of calcareous growth the residual velocity effect results mostly from the mass transfer boundary layer external to the film. In this study an electrochemical system offers the possibility of experimentally monitoring the reaction rate and film growth. The imposed electric fields as a result are expected to be somewhat different than in the electrokinetic phenomena discussed for power plant fouling [2] but the dissimilarities for these two fouling problems may be not as large as one might first expect since in both cases an ionic layer appears next to the surface.

Cathodic phenomena [3] observed at cathodes in an electrolyte solution arise appreciably when there is a significant flow of current. With no current there is an equilibrium between the metal of the cathode and the ions in solution; that is, the rates of metallic dissolution just match those of deposition. Since the passage of cations from an electrode into solution is easier than the reverse, a small buildup of free electrons on the surface results with a corresponding accumulation of positive ions on the solution side of the electrode. This segregation of ions at the cathode surface is termed the "electrical double layer" and the potential difference across this layer is just the individual electrode potential.

In this way the cathode exhibits its reversible potential.

Now with a flow of current a departure from equilibrium results in three molecular processes: the diffusion of ions from the bulk electrolyte to the electrode interface, the recombination of ions with the free electrons at the interface to form atomic species, and the conversion of these atomic species into a stable gaseous, crystalline, or other state. The overall rate of current flow is the net effect of these individual processes. The individual rates depend on various conditions in different ways, so that any one of these processes may become rate controlling under a specific set of conditions. These cathodic phenomena are important in the development of this study.

The current–voltage curve and the diffusion current

For the case when the diffusion process of ions to the cathode is controlling, this condition results in a concentration polarization. That is, there is an appreciable concentration gradient (or activity gradient for concentrated solutions) near the surface. At this point, the problem becomes one of mass transfer and its dependence on hydrodynamics. The layer across which most of the concentration gradient occurs is termed "diffusion layer" in most texts on electrochemistry [3], which is identical to the concentration boundary layer arising in mass transfer.

This concentration polarization increases as the current flux is increased until another cation can discharge, such as hydrogen, whereupon the current will then increase as hydrogen gas is evolved. This limiting current is illustrated in Fig. 1 for the system of pure salt water with a salinity of about 35 ppm. As the voltage applied across the metal-electrolyte interface is increased from zero (the cathode voltage becoming more negative) little current flows until the decomposition voltage is reached: here −0·4 V at 20°C. This critical voltage, where the current suddenly rises, becomes more negative as the temperature is increased, being −0·65 V at 47·8°C. There is

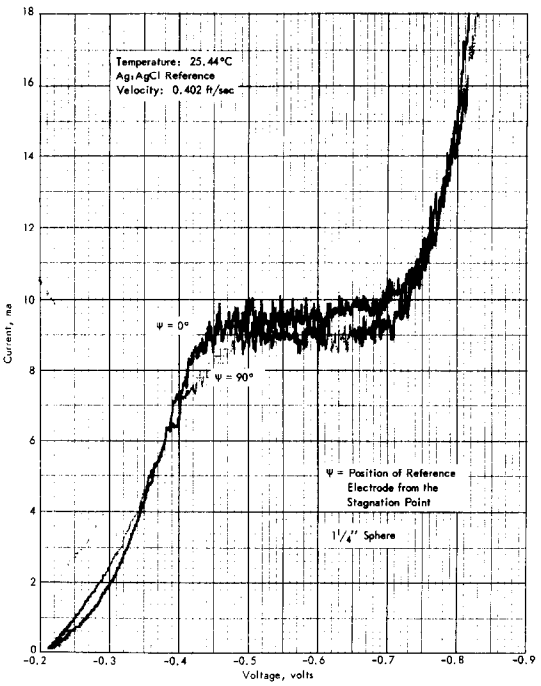

FIG. 1. Current–voltage relation in a salt solution.

apparently no theoretical significance of this voltage, for it is merely that electrical driving force which is necessary to cause appreciable currents to flow. As the voltage applied across the cell is further increased the current increases until the diffusion current of oxygen dissolved in the electrolyte is achieved. At this point the current flow is limited by the rate at which dissolved oxygen can diffuse to the surface, and the voltage applied across the cell can be increased markedly as concentration polarization occurs. The applied voltage can be increased up to a point where the decomposition voltage of hydrogen ions is reached, whereupon hydrogen gas is evolved and the associated current rapidly increases. Actually there is a slight voltage excess on the electrode which is required before visible signs of hydrogen gas evolution are noted. This "overvoltage" is a strong function of the nature of the electrode, and for clean iron the voltages where significant amounts of hydrogen gas are evolved are about 1·1 V at 25°C. This is a qualitative description of the complete current–voltage curve shown in Fig. 1.

The geometry of the electrodes and electrical connections of the various electrodes is shown in Fig. 2. The voltage source together with current and voltage detectors are shown. Voltage

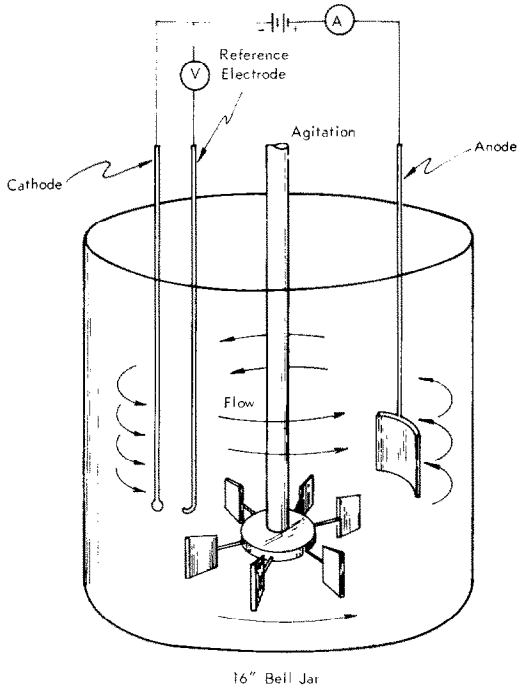

FIG. 2. Geometry and configuration of electrodes.

measurements are made with respect to a Ag:AgCl reference electrode ($E^\circ = -0{\cdot}2224$ V at 25°C). As shown in Fig. 1 the current–voltage curve is not significantly influenced by the position of this reference electrode. The only requirement is that it be placed just outside the concentration boundary layer.

Now that the current–voltage relationships are qualitatively established for the pure salt water system containing dissolved oxygen, let us examine its relation to surface transport and quantitative predictions for a real system. The dissolution rate of a clean iron surface in a salt water electrolyte depends upon the rate at which dissolved oxygen can diffuse to the metal–water interface and become reduced at the surface:

$$4e^- + O_2 + H_2O \rightleftharpoons 4OH^- \quad (1)$$

$$2Fe \rightleftharpoons 2Fe^{++} + 4e^-. \quad (2)$$

Also the dissolved iron can react with the hydroxyl ion to form iron oxide:

$$2Fe^{++} + 4OH^- \rightleftharpoons 2FeO + 2H_2O. \quad (3)$$

When the current required for the reduction of oxygen in equation (1) is supplied not from the iron half-cell reaction in equation (2) but from an external source such as a d.c. power supply then the iron surface is at a constant surface concentration. The current which must be supplied from the source must exactly match the diffusion current arising from the oxygen arrival and in this way exactly supply enough electrons for the reaction in equation (1) and stop the iron dissolution reaction in equation (2). Now it is just this current which we desire to predict quantitatively for modeling heat transfer fouling.

The Sherwood number and limiting current density

The limiting current density can be directly related to the Sherwood number. It can be thought of as the dimensionless concentration gradient at the surface. Now from Fick's law the mass flux of oxygen, N_A, can be related to the concentration gradient, and the mass flux of species can be calculated from the current density:

$$N_A = -\mathscr{D}_{AB}\left.\frac{\partial C_A}{\partial y}\right|_{y=0} = \frac{J}{n\mathscr{F}} \quad (4)$$

where J is the current density (A/cm^2), n is the number of equivalents per mole of oxygen (in this case 4), and the $\mathscr{F}$ is Faraday's constant (96 520 As/ equivalent). The Sherwood number is then just:

$$Sh = \frac{N_A d}{\mathscr{D}_{AB}(C_{A,\infty} - C_{A,0})}. \quad (5)$$

From equation (4) this can be written as:

$$Sh = \frac{Jd}{n\mathscr{F}\mathscr{D}_{AB}(C_{A,\infty} - C_{A,0})}. \quad (6)$$

This simple relation illustrates that the limiting current density that is desired is directly related to a mass transfer parameter, the Sherwood number, which is predictable from the hydrodynamics of the problem.

The concentration of oxygen on the cathode surface must be zero when the reaction is diffusion controlled, since as soon as the oxygen molecule can diffuse to the surface it is instantaneously reacted by equation (1), thus,

$$C_{A,0} = 0. \tag{7}$$

The concentration of dissolved oxygen in the salt water and diffusion coefficient are completely determined once the temperature and salinity are known. Consequently, $\mathscr{D}_{AB}$ and $C_{A,\infty}$ are constants of the system. Equation (6) states that the product of the current density and the diameter of the electrode (idealized as a sphere or cylinder) will be completely determined by the hydrodynamics. This practical result has been tested experimentally in Fig. 3. The current–voltage curves were run for two spherical electrodes of different diameters ($1\frac{1}{4}$ and $\frac{5}{8}$ in.).

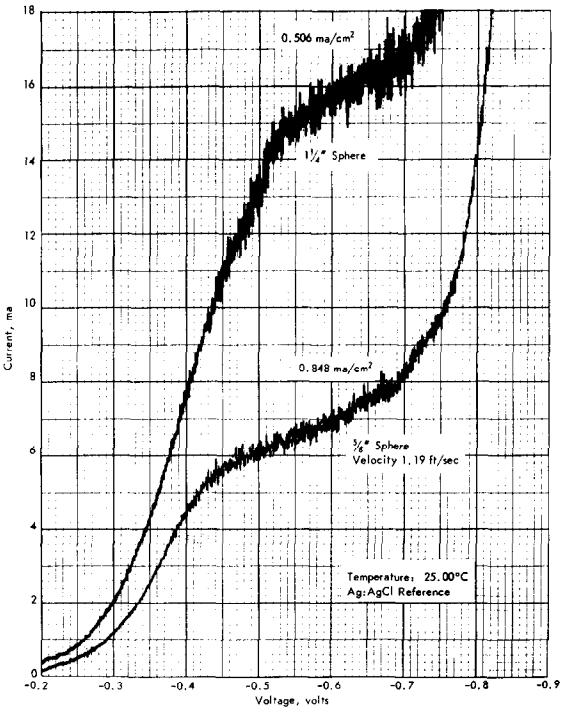

FIG. 4. Effect of sphere diameter on the current–voltage curve at high velocity.

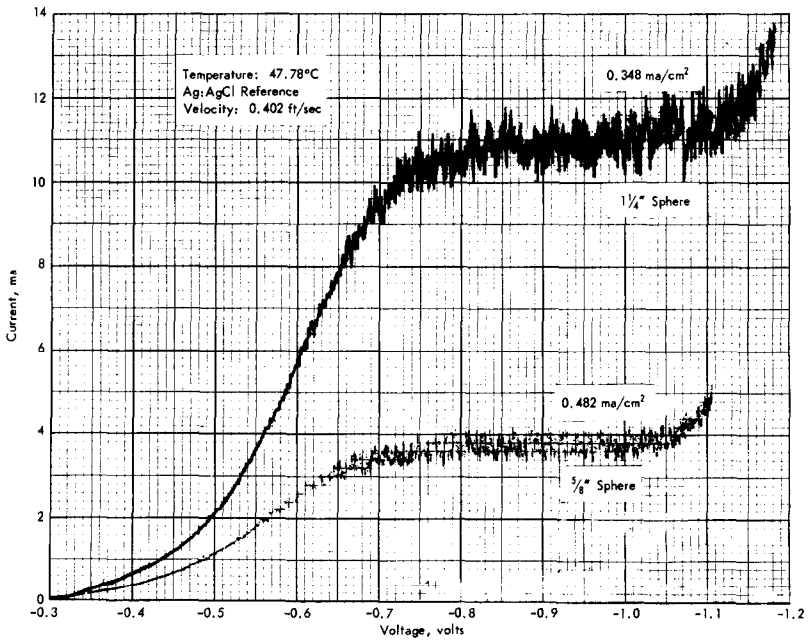

FIG. 3. Effect of sphere diameter on the current–voltage curve at low velocity.

As shown, only the current plateau has shifted. For the same water velocity of 0·402 ft s^{-1} the larger sphere requires less in current densities (0·348 mA/cm^2 compared to 0·482 mA/cm^2). In fact these current densities differ by a factor of the square root of 2. The reason for this is now clear. Since the Frossling number [5] that was discussed earlier is almost invariant, the Sherwood number depends primarily on the square root of the Reynolds number. Now because the Reynolds number involves the diameter, equation (6) that the product of the current density times diameter, Jd, is proportional to the square root of diameter, and thus:

$$J \propto d^{-\frac{1}{2}}. \tag{8}$$

This relation is also approximately true at higher velocities as illustrated in Fig. 4. This dependence of current density on diameter can be important in the design of a variety of optimized shell and tube heat exchanger tube bundles and will be discussed later.

Experimental Frossling numbers

First, let us examine the invariant nature of the Frossling number. Earlier it was shown [4–7] that the Frossling group decreased from near unity at the forward stagnation to a minimum value near 90° where separation of the boundary layer occurred. In the wake-flow region behind the sphere the Frossling number has been studied experimentally [6]. The magnitude of the Frossling number was shown to be significantly enhanced near the forward stagnation point as a result of increased free stream turbulence in the flowing stream.

The actual dependence of the Frossling number on the angle from stagnation, the Reynolds number, Schmidt number, and free stream turbulence is known. The total current density required by a cathode is the surface average of the local current requirements that are a function of angle. The diffusion current shown in Figs. 3 and 4 is a surface average and can be predicted from the surface average Frossling

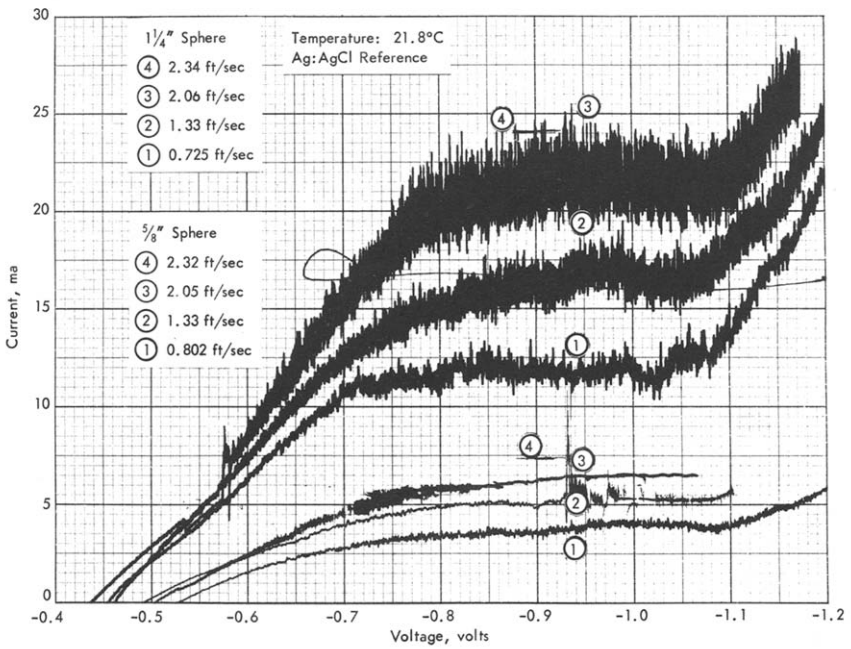

FIG. 5. Effect of diameter and velocity on the diffusion current.

number. A number of diffusion currents were determined over a range of velocities, turbulence levels, and temperatures, such as illustrated in Fig. 5. From these current densities a Sherwood number was calculated from equation (6). The fluid velocity was measured with a conventionally designed pilot tube, and from this velocity the Reynolds number was calculated. Knowing the temperature of the fluid establishes the Schmidt number.

Table 1. Experimental Frossling numbers

Test no.	Date 1967	Temp. °C	*Re*	*I**	*Sc*	*Sh*†	*Fs*	Notes
1	4/7	—	—	—	—	—	—	Pt and Fe test coupons
2	4/7	20	300	0·05	506	—	—	Dirty 11/4 in. sphere
3A‡	4/7	20	300	0·05	506	107·8	0·763	Uninsulated stem
3B	4/7	20	150	0·05	506	124·8	1·229	Uninsulated stem
4A	4/7	20	300	0·05	506	83·4	0·591	Insulated stem
4B	4/7	20	150	0·05	506	67·6	0·667	Insulated stem
5A	4/7	20	3870	0·1	506	552	1·110	Insulated stem permanent
5B	4/7	20	3500	0·1	506	420	1·168	
6A	4/10	23·1	96·3	0·05	416	44·4	0·58	No stirring
6B	4/10	23·1	36	0·05	416	28	0·58	Velocity by timing particles
7A	4/10	23·1	4310	0·1	416	518	1·053	
7B	4/10	23·1	2155	0·1	416	342	0·982	
8A	4/11	22·8	8400	0·2	416	564	0·82	Poor velocity
9	4/11	27·8	—	—	—	—	—	Platinized test
10A	4/11	47·7	17900	0·2	59·4	539	1·025	Heated
10B	4/11	47·7	8900	0·2	59·4	374	1·008	Heated
11A	4/12	25·0	4600	0·1	395	652	1·296	Ref electrode position was varied as test
11B	4/12	25·0	2320	0·1	395	438	1·232	
12A	4/12	25·4	4620	0·1	395	638	1·270	
13A	4/12	25·0	11780	0·3	395	1116	1·40	
13B	4/12	25·0	6890	0·2	395	984	1·60	
14A1	4/12	25·0	17620	0·2	395	1340	1·373	
14A2	4/12	25·0	13200	0·3	395	955	1·129	
14B	4/12	25·0	9442	0·2	395	1116	1·56	
15B	4/12	25·1	5890	0·2	395	745	1·318	Also test/1 day rust
16B1	4/12	24·6	8930	0·3	395	1077	1·55	
16B2	4/12	24·6	7550	0·3	395	1000	1·56	
16B3	4/12	24·6	5490	0·2	395	837	1·53	
16B4	4/12	24·6	4810	0·2	395	744	1·46	
16B5	4/12	24·6	2840	0·2	395	571	1·45	
16B6	4/12	24·6	3490	0·2	395	638	1·46	
17A	4/12	—	—	—	—	—	—	Poor plateau
18B	4/13	22·2	—	—	—	—	—	Sea water/film growth
19A	4/13	22·2	—	—	—	—	—	Sea water/film growth
20A1	5/31	21·8	23900	0·2	454	1476	1·235	Pure salt water
20B1	5/31	21·8	11870	0·2	454	890	1·06	
20A2	5/31	21·8	21000	0·2	454	1320	1·18	
20B2	5/31	21·8	10500	0·2	454	783	0·995	
20A3	5/31	21·8	13570	0·2	454	1020	1·142	
20B3	5/31	21·8	6780	0·2	454	624	0·985	
20A4	5/31	21·8	7380	0·2	454	724	1·09	
20B4	5/31	21·8	4080	0·1	454	452	0·917	
21 ⋮ 41								Film growth studies

* Turbulence intensity estimated from observation of particle motions.
† For spheres the molecular diffusion limit of 2 was subtracted.
‡ A denotes $1\frac{1}{4}$ in. sphere, B denotes $\frac{5}{8}$ in. sphere.

Once these three dimensionless groups were obtained, the Frossling number was calculated from the definition $[Fs = (Sh - 2)/Re^{\frac{1}{2}}Sc^{\frac{1}{3}}]$. These values have been compiled in Table 1. Tests 1–20 were carried out in pure salt water with a salinity of about 35 ppm. These data have been shown in Fig. 6 together with available data [4–6] for spheres and cylinders. The solid curves represent an average of the least squares curves established for spheres [5] and cylinders [4]. At a critical Reynolds number of 2×10^5 for the lowest turbulence involved there is an abrupt change in the dependence of the Frossling number. This critical Reynolds number decreases with increased turbulence. The physical significance of this transition is that the laminar boundary layer which develops on the front portion of the sphere evolves into a turbulent boundary layer before it separates from the surface at about 90°. This transition discussed [7] and has been experimentally established from pressure profile measurements [8] and heat transfer [4,5]. When the Reynolds number is above this critical value (termed "supercritical") the effects of turbulence seem to be less important. The quantitative damping of the effects of turbulence in supercritical flow is not well established and more work needs to be done in this area. Also the residual dependence of the Frossling number on the Schmidt number (or Prandtl number for heat transfer) needs to be refined. This weak dependence was found to be necessary to bring together transport data for heat transfer and mass transfer and for gases and liquids based on regression analysis of a large amount of experimental data [4–5]. Accepting these results leads one to the plot of Fig. 6 involving the empirical $Sc^{\frac{1}{3}}$. The kinematic viscosity ratio between the surface and free stream, ν_0/ν_∞, arises from weak effects of variable physical properties through the boundary layer on the fluid mechanics. The experimental data taken with the $1\frac{1}{4}$ in. and the $\frac{5}{8}$ in. spherical electrode are in reasonable agreement with the previously established curves. The experimental set-up using an impeller to generate the flow

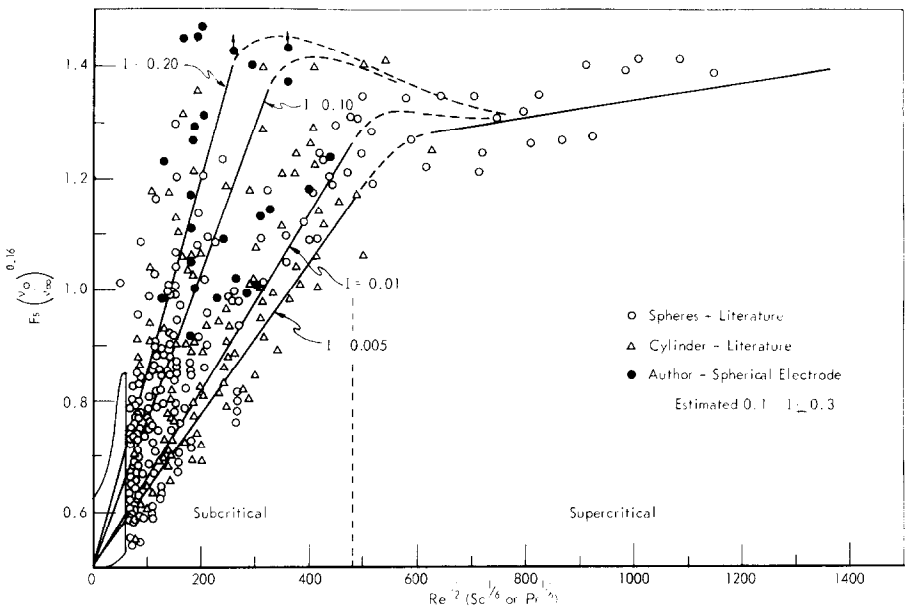

FIG. 6. Surface average Frossling number for a clean cylindrical or spherical surface.

in a battery jar by necessity creates a high intensity of turbulence. Several impeller configurations were used to obtain these data and the turbulence generated varied for the different configurations. Generally the lower data were obtained with a radial flow impeller with six small paddles and driven by an air motor applying constant torque. Estimates of the turbulence intensity are required for more quantitative comparisons with literature work.

2. CALCAREOUS FILM DIFFUSION BARRIER

Now that the current requirements for a clean surface can be predicted from a knowledge of hydrodynamics, let us examine the complication of a diffusion barrier or "dirty" surface. When dissolved oxygen diffuses to the surface it undergoes reaction to form hydroxyl ion as discussed earlier in equation (1). In sea water there are small concentrations of metallic ions such as calcium and magnesium which will react with the hydroxyl ion on the surface and eventually form a somewhat crystalline film (termed "calcareous") which acts as a barrier to the diffusion of oxygen to the iron surface of the electrode. A long term goal of this project is to eventually understand the chemical and structural nature

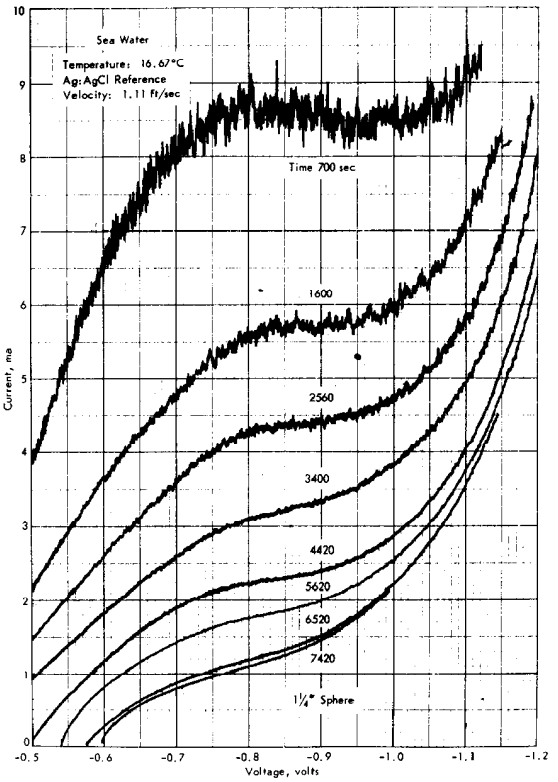

FIG. 7. Current–voltage curves in sea water.

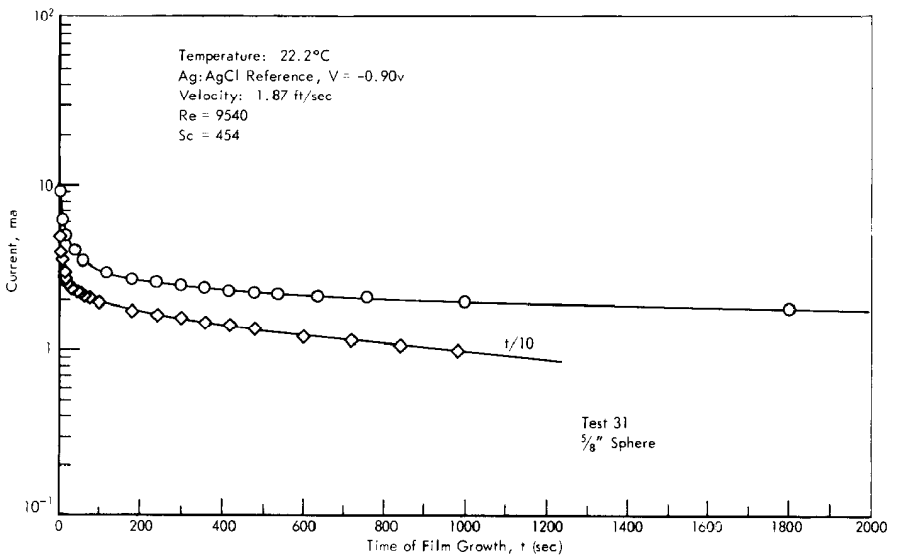

FIG. 8. Decay of the diffusion current.

of this film, but at the present it is only necessary to first describe the rate of film growth and complications of hydrodynamics.

A current–voltage relationship measured as before in the electrolyte system, sea water, differs significantly from the pure salt water electrolyte. As shown in Fig. 7 the diffusion current decays with time. As soon as the clean iron surface is placed in the sea water and under cathodic protection, the diffusion barrier or calcareous film begins to grow. It forms very rapidly at first and rapidly slows to a rather steady rate. The rate of decay is much stronger than exponential as shown in Fig. 8. The actual shape of the decay will be developed.

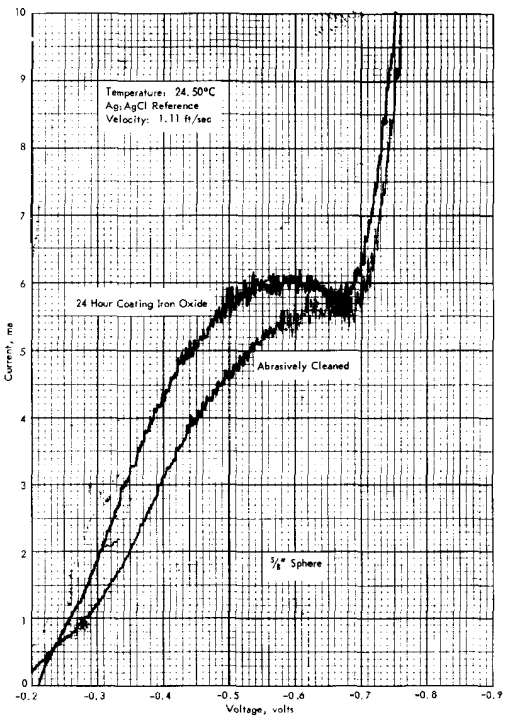

FIG. 9. Reduction of oxide film.

This diffusion barrier is not to be confused with an oxide film which will form immediately on a clean iron surface placed in sea water when the surface is not under cathodic protection. During the short period between placing the iron specimen in the sea water and adjusting the voltage to achieve cathodic protection, this oxide film will form. When the specimen is put under control this oxide film will be electrochemically reduced. Additional current is required to carry out this reduction as shown in Fig. 9. The oxide film was formed by heating the specimen in a furnace for 24 hours. This effect is easily distinguishable from the diffusion barrier effect.

The effective Sherwood number

The presence of a diffusion barrier which is an electrical insulator significantly reduces the diffusion current, and thus the effective Sherwood number computed from this current is reduced. The magnitude of this reduction can be derived from a species balance on a cylindrical surface for steady state diffusion with no chemical reactions away from the surface:

$$\frac{\mathrm{d}}{\mathrm{d}r} r\left(\frac{J}{n\mathscr{F}}\right) = 0 \tag{9}$$

where the nomenclature is identical to that used previously. If the subscript 0 denotes the surface, 1 outside the diffusion barrier and ∞ outside the concentration boundary layer then there obtains:

$$r_0\left(\frac{J_0}{n\mathscr{F}}\right) = r_1\left(\frac{J_1}{n\mathscr{F}}\right) = r\left(\frac{J}{n\mathscr{F}}\right) = -\mathscr{D}_{0_1} r\left(\frac{\mathrm{d}C_A}{\mathrm{d}r}\right). \tag{10}$$

The last equality is Ficks law. The concentration difference across the barrier is:

$$C_{A,1} - C_{A,0} = r_0\left(\frac{J_0}{n\mathscr{F}}\right)\left[\frac{\ln(r_1/r_0)}{\mathscr{D}_{0_1}}\right] \tag{11}$$

and the concentration difference across the concentration boundary layer is obtained from the definition of the mass-transfer coefficient, k_A, and equation (10);

$$C_{A,\infty} - C_{A,0} = J_0\left[\frac{r_0}{n\mathscr{F}}\left(\frac{1}{r_1 k_A} + \frac{\ln(r_1/r_0)}{\mathscr{D}_{0_1}}\right)\right]. \tag{13}$$

Since the Sherwood number based on the clean surface is just $2r_0k_A/\mathscr{D}_\infty$ equation (13) can be written as:

$$\frac{J_0 2r_0}{n\mathscr{F}\mathscr{D}_\infty(C_{A,\infty} - C_{A,0})} = \frac{1}{\frac{1}{Sh} + \frac{\mathscr{D}_\infty \ln(r_1/r_0)}{2\mathscr{D}_{0_1}}}. \quad (14)$$

This group on the left can be termed as the "effective Sherwood number", Sh_{eff}, and the group, $1/2\ln(r_1/r_0)$, can be taken as the dimensionless film thickness, ξ. For thin films this thickness, ξ, is just the film thickness, δ, divided by the sphere diameter, d. Equation (14) can be written:

$$Sh_{\text{eff}} = \frac{1}{\frac{1}{Sh} + (\mathscr{D}_\infty/\mathscr{D}_{0_1})\xi}. \quad (15)$$

The known dependence of the Sherwood number for a clean surface upon the Reynolds number, Schmidt number, and turbulence levels of the flow, as shown in Fig. 6, can be used in this relationship to predict the effective Sherwood as in Fig. 10. Note that at high Reynolds numbers and large film thicknesses the rate of mass transfer is completely controlled by the diffusion barrier that is, the Sherwood number becomes independent of the Reynolds number as in Fig. 10.

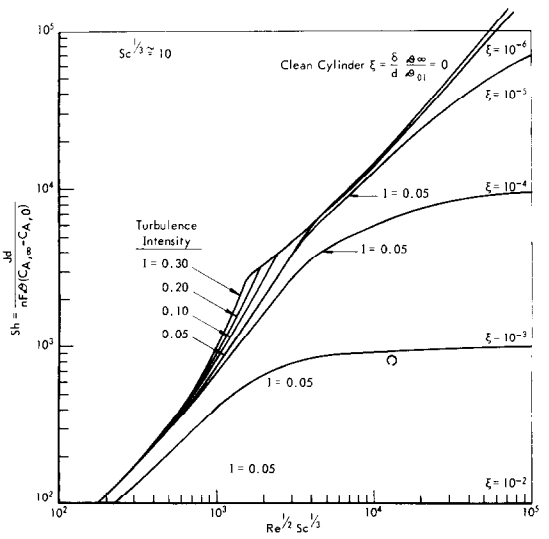

FIG. 10. Diffusion barrier and the effective Sherwood number.

The fouling resistance on the outside surface, R_{f_0}, is defined as $k_{\text{eff}}^{-1} - k_0^{-1}$ for mass transfer and $U^{-1} - h_0^{-1}$ for heat transfer. In this work the growth law of the film thickness, δ, is developed. To obtain the fouling resistance, R_{f_0}, one divides the film thickness, δ, by either the effective diffusivity of the mobile species within the film or the effective thermal conductivity of the film. Generally the latter quantity is known to considerably better accuracy than is the film thickness.

3. CALCAREOUS FILM GROWTH MODEL

The predictions developed so far required a knowledge of the diffusion barrier created by the calcareous film, the physical structure of the film, the rate of growth, and the coupling effects with hydrodynamics. In this section these features of the film are studied and made quantitative.

Experimental evidence

In Fig. 11 there are shown the effects of the diffusion barrier on the effective Frossling number obtained from Fig. 10. Such a plot enlarges the region where the diffusion barrier is controlling. The solid points are those data that were obtained by D. M. Seid and the author using a clean spherical electrode. As discussed earlier these data are in substantial agreement with other authors. Several intriguing experiments are shown in this figure which illustrates the complicated properties of this diffusion barrier.

The reaction product of oxygen at the electrode surface, hydroxyl ion, reacts with the magnesium and calcium ions in the sea water in a proportion which depends upon the solution pH and the bicarbonate ion concentration. A concentration gradient of hydroxyl ion would prevail at the surface and depend directly upon the rate of oxygen transfer,

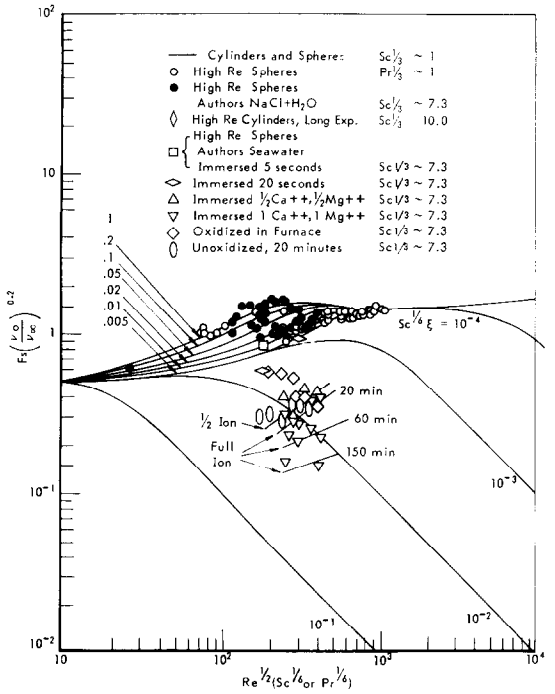

FIG. 11. Diffusion barrier and the effective Frossling number.

however, this picture is complicated by hydroxyl reaction with these metallic ions near the surface which drastically steepens this profile. The ability of the metallic ions and hydroxyl ions to react is indicated by their associated solubility product. The rate at which the metallic ions diffuse to the surface and the hydroxyl ions diffuse away depends upon the hydrodynamics. When the product of the concentrations of these two ions exceeds the solubility product, a solid precipitate can nucleate on a suitable surface. In a relatively clean system the solid deposit nucleates on the nearby electrode surface. At high current densities, like those for a clean surface, the principal deposit is magnesium hydroxide with somewhat less carbonate [9].

An experiment in pure salt water, saturated with carbon dioxide in equilibrium with the atmosphere, was done using the clean spherical electrode and plotting the current voltage curve for various additions of ionic components of sea water. Between each addition the electrode surface was cleaned. At the high current

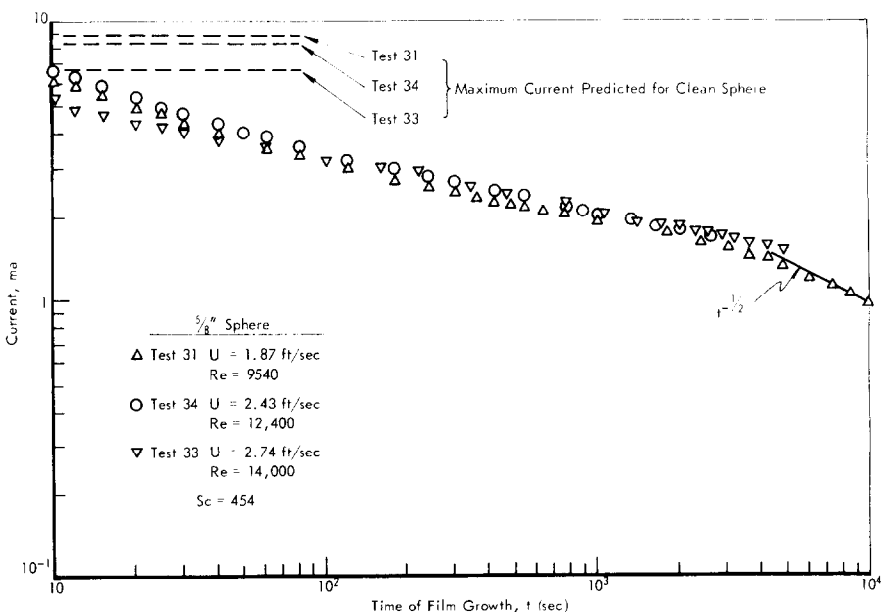

FIG. 12. Measured surface average current decay for $\frac{5}{8}$ in. sphere.

densities associated with a clean surface the magnesium ion was found to cause the calcareous deposit to form, whereas additions of calcium did not. The calcium was found to participate in film growth only in electrolytes of high pH. When a film was deposited, bicarbonate ion had the effect of dissolving a portion of the film and increasing initially the current density requirements. Varying the bicarbonate ion concentration during any period of film growth affected the current densities directly. The experiments illustrated the complicated role of electrolyte pH and bicarbonate ion in the mechanism of film deposition.

The growth of this film over relatively long periods and hydrodynamic coupling was studied in a series of experiments in sea water with the two spherical electrodes ($1\frac{1}{4}$ and $\frac{5}{8}$ in. dia.) held at $-0{\cdot}85$ V relative to a reference electrode. The data points shown in the center of Fig. 11 illustrates the effect of film growth upon the Frossling group for various exposure times. The triangular points shown were taken with the film grown on the spherical electrode subjected to a constant velocity. The films grown at the higher velocities offered the least resistance, but this effect rapidly decreased with increased exposure. Note that these data cross the solid curves for constant values of the dimensionless film thickness, ξ. These curves represent the effect of a series resistance to diffusion with the calcareous film taken to be the predominate diffusion barrier. Thick films offer high barriers, and these correspond to a Sherwood group which is independent of the Reynolds number or a Frossling number inversely proportional to the square root of the Reynolds number.

The oval points shown were taken with the electrodes subjected to a constant velocity and the current measured after film growth for 20 min. Then the velocity was sharply increased and the current measured. Finally, the velocity was decreased and the current measured again. These data cross those discussed above. For this case the diffusion barrier is nearly held at a constant resistance (the structure does not change) and only the velocity outside this film is varied. Note that this case conforms with the model as shown by the solid curves for constant

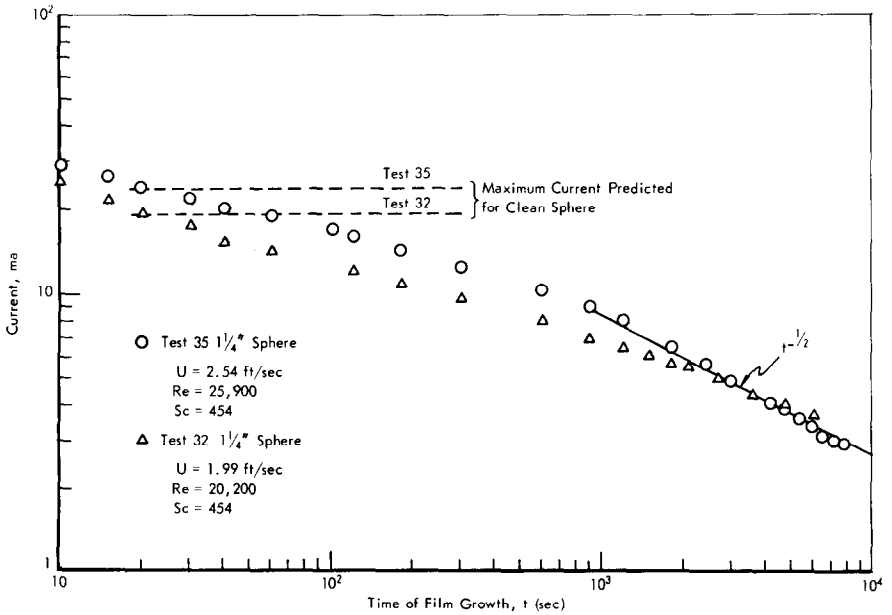

FIG. 13. Measured surface average current decay for $1\frac{1}{4}$ in. sphere.

film thickness. These experiments illustrate the effects of hydrodynamics in the growth mechanism of the calcareous films.

The growth rate of this film over a long period of time was studied in a series of experiments using the $\frac{5}{8}$ and $1\frac{1}{4}$ in. iron spheres. The results for the surface average current are shown in Fig. 12 for the $\frac{5}{8}$-in. sphere and Fig. 13 for the $1\frac{1}{4}$ in. sphere. A log–log plot of current versus time was chosen for the display of the data to emphasize the initial, hydrodynamically dependent portion and the approach to the $t^{-\frac{1}{2}}$ law. The actual shape of these curves will be made quantitative but first let's examine the experimental evidence. In these figures the velocity was varied and a close examination of the data illustrates slight variations in absolute magnitude. The maximum current required for the clean surface has also been shown in these figures to illustrate the magnitude of the velocity effect. Besides this effect at short times there is a velocity effect in the approach to the diffusion barrier controlled limit shown by the $t^{-\frac{1}{2}}$ line.

Local mass transfer limited film growth

The prediction of the shape of the surface average current decay curves quantitatively requires an analysis to be made taking into account the local variation on the surface as the film grows. If the diffusion barrier model developed in equation (15) is used, and it is assumed that all of the hydroxyl formed reacts with either magnesium or calcium ions in the sea water and the precipitate is deposited on the surface, then a species balance becomes:

$$\frac{N_A d}{C_{A,\infty}} = \frac{1}{\dfrac{1}{\mathscr{D}_\infty Sh} + \dfrac{\xi}{\mathscr{D}_{01}}} = \frac{\rho d^2}{C_{A,\infty}} \frac{d\xi}{dt}. \qquad (16)$$

The quantity, ρ, is the density of the solid calcareous film on the surface. The quantity, N_A, is the molar flux of oxygen, which is also numerically equal to the flux of hydroxyl ions when the surface is under cathodic protection. In other words $(d\xi/dt)d$ is analogous to the velocity that the film surface is traveling as it grows away from the clean surface. Note that in an actual case the film is being removed at a small rate by dissolution (which is influenced by mass transfer), abrasion, or by hydrogen gas evolution scouring. The film dissolution will show up for long times and will have the effect as to creating a lower asymptote to which the current will approach at very large times.

The solution to equation (16) can be obtained using the boundary condition that $\xi = 0$ at zero time as follows:

$$\xi = \sqrt{\left[\frac{2\mathscr{D}_{01} C_{A,\infty}}{\rho d^2} t + \left(\frac{\mathscr{D}_{01}}{\mathscr{D}_\infty} \frac{1}{Sh}\right)^2\right]} - \frac{\mathscr{D}_{01}}{\mathscr{D}_\infty} \frac{1}{Sh}. \qquad (17)$$

This expression gives the dimensionless film thickness, which for thin films is just the actual film thickness divided by the cylinder or sphere diameter, d, as a function of the hydrodynamic variables, fluid and film properties, and time of surface exposure. This can then be substituted into equation (15) for the effective Sherwood number:

$$\frac{Jd}{n\mathscr{F}\mathscr{D}_\infty C_{A,\infty}} = \frac{1}{\sqrt{\left[\left(\dfrac{2\mathscr{D}_\infty C_{A,\infty}}{\rho d^2}\right)\left(\dfrac{\mathscr{D}_\infty}{\mathscr{D}_{01}}\right) t + \left(\dfrac{1}{Sh}\right)^2\right]}}. \qquad (18)$$

This result predicts the actual current decay as a function of the same variables.

The local current density

At the forward stagnation point of a $1\frac{1}{4}$ in. sphere in sea water ($Sc = 665$) flowing with a Reynolds number of 21000 and turbulence level of 7·5 per cent the Sherwood number is about 1515. For this case a set of predictions were made for various diffusivity ratios in Fig. 14. The more oxygen impenetrable is the calcareous deposit the faster the current decays.

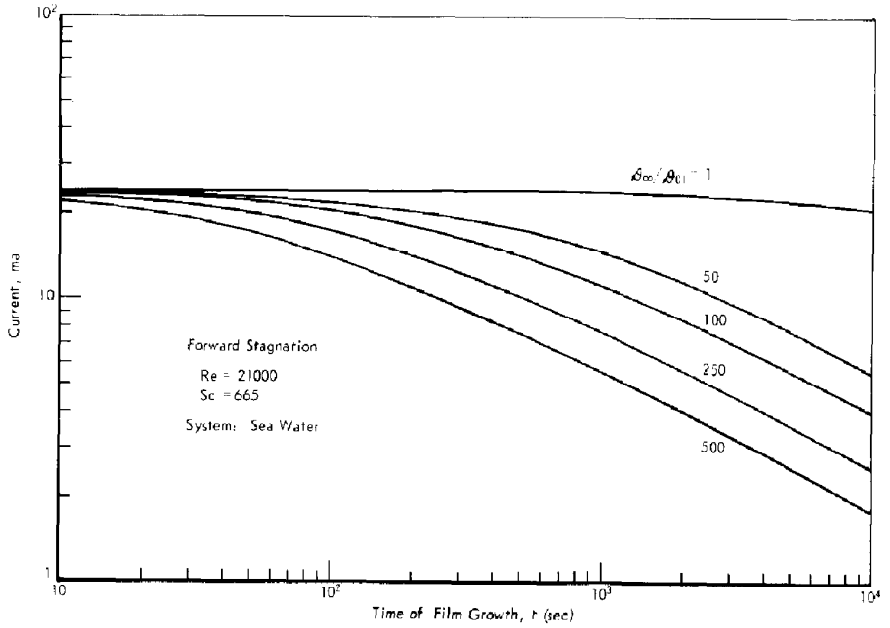

FIG. 14. Predicted time decay of electrical current requirement for cathodic protection of the forward stagnation on $1\frac{1}{4}$ in. sphere.

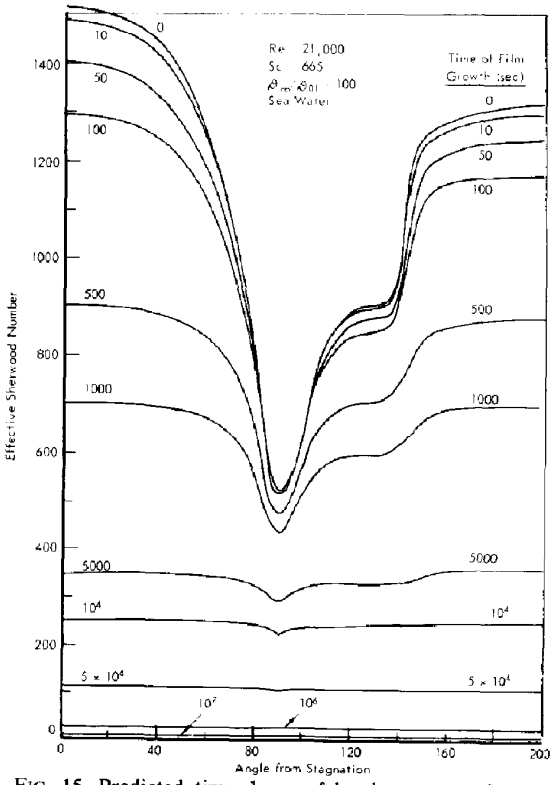

FIG. 15. Predicted time decay of local mass-transfer rate around a $1\frac{1}{4}$ in. sphere.

If this computation is repeated using the entire local variation of the Sherwood number, the current decay can be predicted at different positions on the surface as shown in Fig. 15. For this case a diffusivity ratio of 100 was chosen. Note that after 10000 s (2·8 h) the local variation of current over the surface has essentially disappeared. This clearly illustrates the "self-compensating" nature of the film; that is, the calcareous film goes where it is the thinnest.

The surface averaged current density

The local variation of current can now be integrated over the surface to obtain the surface average current as a function of time. This has been done in Fig. 16. Note that after 10000 s the diffusion barrier limit is reached as indicated by the $t^{-\frac{1}{2}}$ law. A comparison has been made for Test 35 in Fig. 17 using a diffusivity ratio of 250. This ratio was selected from the best fit of the data. Eventually from a knowledge of the physical structure of the calcareous crystalline film it is hoped that this ratio can be predicted quantitatively. The majority of the minor fluctuations of the data in this figure arise principally from

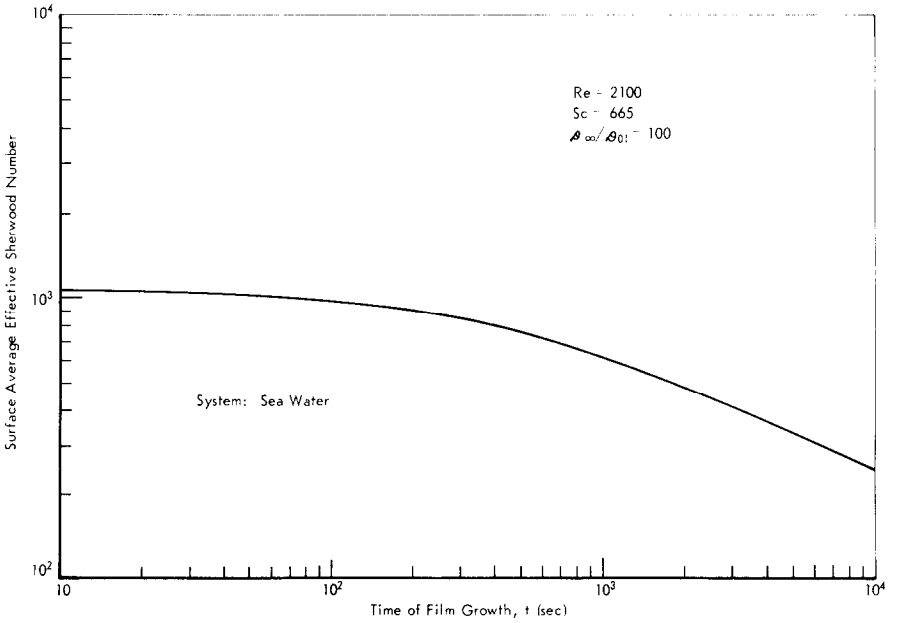

FIG. 16. Predicted time decay of surface average effective Sherwood number for $1\frac{1}{4}$ in. sphere.

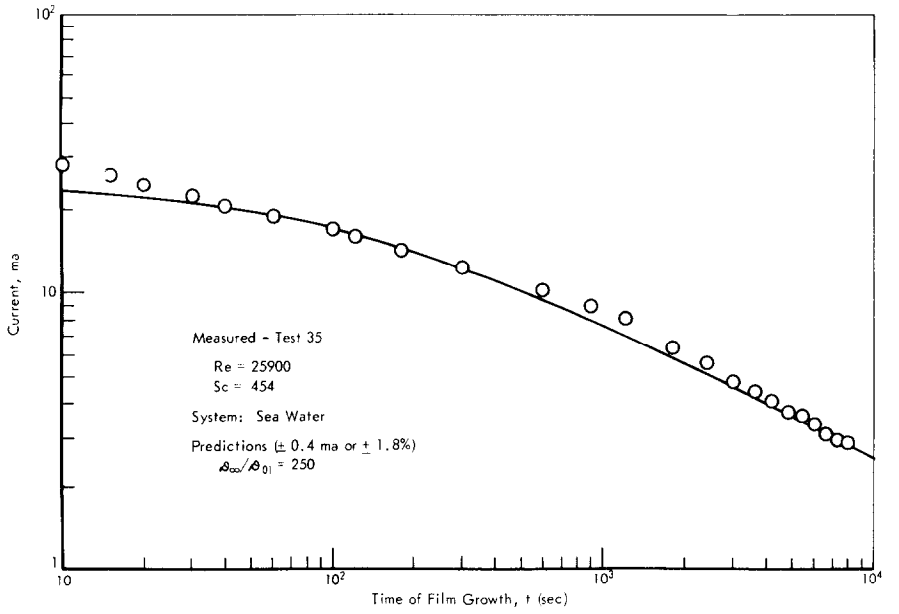

FIG. 17. Measured and predicted surface average current decay for $1\frac{1}{4}$ in. sphere.

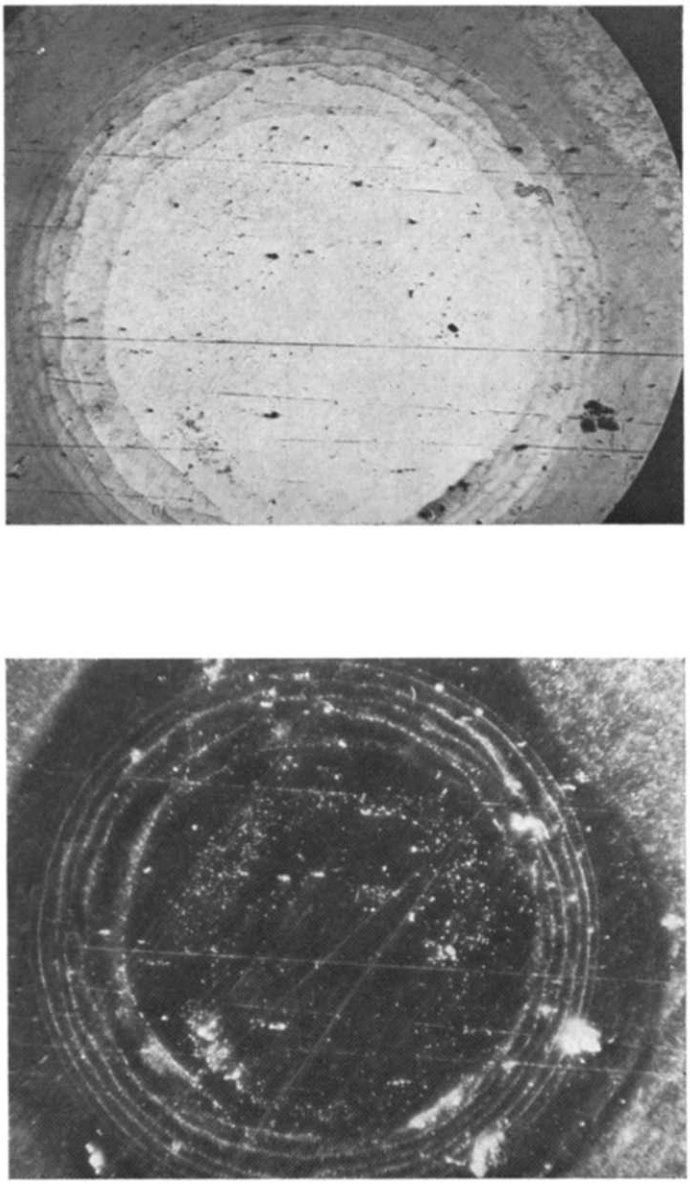

FIG. 19. Photomicrographs of calcareous deposit grown for 2 h.
Top: Light field—Scale 80 000 A/mm.
Bottom: Dark field—Scale 80 000 A/mm.

[*facing page 458*]

the fluctuations in the outer velocity as a result of the method of stirring.

Figure 18 shows the film growth results. In most cases the actual film thickness is such a small fraction of the sphere diameter (0·25 μ in 2 h) as it was found to be invisible. Only when

CONCLUSIONS

A model has been developed for the growth rate of calcareous films in terms film thickness as a function of time, geometry and fluid mechanics. The growth law was verified by confirming electrochemical experiments involving oxygen

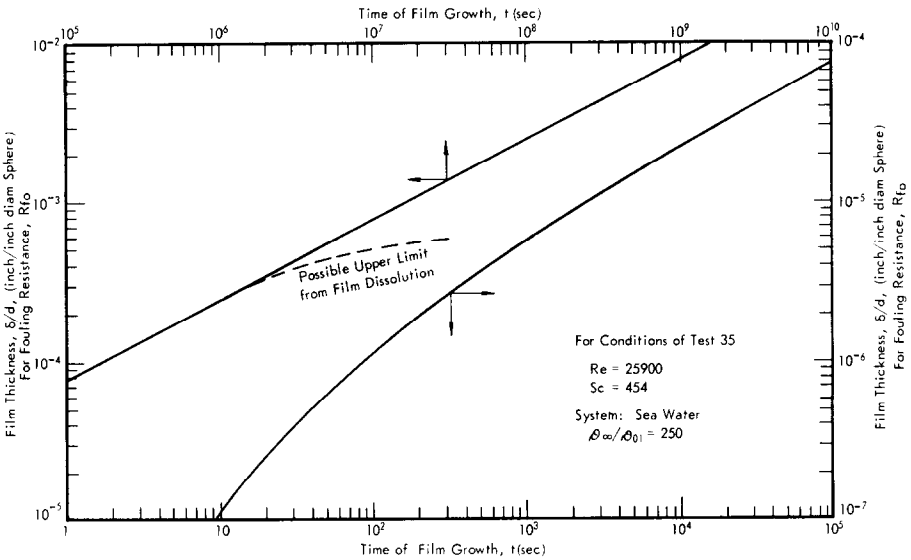

FIG. 18. Predicted fouling resistance from surface average growth of calcareous film on $1\frac{1}{4}$ in. sphere.

the surface was dried and light was reflected off could a white cast be detected. In Fig. 19 two photomicrographs are shown of a surface with calcareous deposits grown for 2 h at a Reynolds of about 20000. This was a flat steel $\frac{1}{16}$ in. specimen, $\frac{3}{4} \times 4$ in. The circular pattern was produced as a result of an air bubble or foreign particle lodged on the surface, with the film growing underneath. Both photos were taken at a scale of 80000 Å mm^{-1} of distance on the photo, or 126 ×. The top one was taken of the surface being directly illuminated whereas the bottom was using a dark field. Although direct quantitative comparisons between a flat specimen and a sphere are not possible, a film thickness of 0·25 μ, would correspond to 0·3 mm on these photos. Judging the height of the crystalline steps to be of the order of 0·1 mm or 8000 Å, it is felt that the predicted thicknesses are of the right order of magnitude.

and salt water. For heat transfer fouling the fouling resistance, R_{fo} can be obtained by dividing the thickness δ' by either diffusivity or conductivity, taken as effective values within the film. One must be careful to apply this growth law to fouling mechanisms (e.g. crystallization, deposition, reaction, etc.) where deposit is formed as a result of the transported component, diffusing through the barrier and reacting with a component appearing at the surface in excess.

ACKNOWLEDGEMENTS

D. M. Seid assisted in the experimental measurements and J. M. Elliott constructed much of the apparatus and their assistance is gratefully acknowledged.

REFERENCES

1. J. TABOREK *et al.* Fouling—the major unresolved problem in heat transfer, Parts I and II. A.I.Ch.E. preprint No. 7, presented at the 12th National Heat Transfer Conference, A.I.Ch.E.-A.S.M.E., Tulsa, Oklahoma, August 15–18 (1971).

2. R. GASPARINI, C. DELLA ROCCA and E. IOANNILLI, A new approach to the study and prevention of deposits in modern power stations, *Combustion Lond.*, 12 18 (November 1969).
3. S. GLASSTONE, *An Introduction to Electrochemistry*. Van Nostrand, Princeton (1960).
4. T. R. GALLOWAY and B. H. SAGE, Local and macroscopic transport from a 1·5 in. cylinder in a turbulent air stream, *A.I.Ch.E. Jl* **13**, 563–570 (1967).
5. T. R. GALLOWAY and B. H. SAGE, Thermal and material transfer from spheres. Prediction of local transport, *Int. J. Heat Mass Transfer* **110**, 539–549 (1968).
6. T. R. GALLOWAY and B. H. SAGE, Local and macroscopic thermal transport from a sphere in a turbulent air stream, accepted by *A.I.Ch.E. Jl.*
7. T. R. GALLOWAY, Solutions of turbulent boundary layer equations for the interaction of free stream turbulence with stagnation flow heat and mass transfer, submitted to *J. Heat Transfer*.
8. H. SCHLICHTING, *Boundary Layer Theory*. McGraw-Hill, New York (1960).
9. R. A. HUMBLE, Cathodic protection of steel in sea water with magnesium anodes, *Corrosion* **4**, 358–370 (1948).

DETERIORATION DU TRANSFERT THERMIQUE PAR LA CROISSANCE D'UN DEPOT CALCAIRE EN FILM

Résumé—La salissement de la surface d'un équipement thermique a pour conséquence un surdimensionnement de l'ordre de 30 pour cent. Ce supplément de métal et de taille coûtent aux Etats-Unis environ 400 millions de dollars par an. En conséquence il y a là une raison importante d'estimer la croissance des dépôts ou des films sur les surfaces.

La croissance des dépôts calcaires sur les surfaces métalliques est estimée en appliquant les principes fondamentaux de la mécanique des fluides et du transfert massique par convection forcée d'oxygène dissous dans de l'eau. L'épaisseur du film est la variable la plus importante qui affecte le taux de transport pariétal et la distribution de croissance. On prend comme modèle le cas idéalisé d'un cylindre maintenu à une concentration superficielle constante avec une barrière de diffusion en série avec la couche limite de concentration. Expérimentalement la croissance avec le temps de la barrière de diffusion et les effets hydrodynamiques supplémentaires ont été étudiés en laboratoire au moyen d'électrodes sphériques placées dans un écoulement d'eau de mer. Ce modèle est utilisé pour estimer la décroissance du courant mesuré expérimentalement.

VERSCHLECHTERUNG DES WÄRMEÜBERGANGS DURCH SALZARTIGE ABLAGERUNGEN IN DÜNNEN SCHICHTEN

Zusammenfassung—Die spätere Verschmutzung der Wärmeübertragungsflächen bedingt ein Überdimensionierung um ca. 30 Prozent. Die zusätzliche Grösse und das zusätzliche Material kosten die Vereinigten Staaten jährlich ca. 400 Millionen Dollar. Es besteht deshalb die Notwendigkeit einer besseren Bestimmung des Anwachsens von Ablagerungen oder Schichten auf den Flächen.

Das Anwachsen kalkhaltiger Ablagerungen auf den Metallflächen lässt sich durch Anwendung der grundlegenden Prinzipien der Strömungsmechanik und durch den erzwungenen konvektiven Stofftransport von gelöstem Sauerstoff in Wasser bestimmen. Die Schichtdicke war die einzige wichtige variable Grösse, die die zur Fläche transportierte Menge und das Anwachsen der Schicht beeinflusste. Es wird der idealisierte Fall eines blanken Zylinders als Modell herangezogen. An seiner Oberfläche wird die Konzentration konstant gehalten mit Hilfe einer Diffusionsbarriere auf Grund der Konzentration in der Grenzschicht. Experimentell wurden das Anwachsen der Diffusionsbarriere mit der Zeit und die komplizierten Effekte der Hydrodynamik an Kugelelektroden in Meerwasser untersucht. Das Modell wird benutzt, um den experimentell gemessenen Stromabfall vorauszubestimmen.

ОБРАЗОВАНИЕ ИЗВЕСТКОВЫХ ПЛЕНОЧНЫХ ОТЛОЖЕНИЙ НА ПОВЕРХНОСТИ ТЕПЛОПЕРЕНОСА

Аннотация—Загрязнение теплообменных поверхностей установок ведет к завышению их размеров при проектировании примерно на 30%, что ежегодно обходится Соединенным Штатам в 400 миллионов долларов. Следовательно, имеется необходимость в лучшем теоретическом определении роста отложений или пленок на поверхностях.

Рост известковых отложений на металлических поверхностях рассчитывается по основным законам механики жидкости и переноса массы растворенного в воде кислорода при вынужденной конвекции. Толщина пленки является единственной важной переменной, определяющей скорость переноса на поверхности и распределение приращения отложений. Рассмотрена идеализированная модель: не покрытый пленкой цилиндр с постоянной концентрацией на поверхности и диффузионным барьером, расположенным последовательно с концентрационным пограничным слоем. Используя сферические электроды, помещенные в текущую морскую воду, в лабораторных условиях экспериментально изучались рост диффузионного барьера со временем и влияние на него гидродинамики. Модель используется для теоретического расчета экспериментально замеренного затухания потока.